Solar Energy Materials & Solar Cells 215 (2020) 110663

Contents lists available at ScienceDirect

Solar Energy Materials and Solar Cells

journal homepage: http://www.elsevier.com/locate/solmat

Potential scalability of a cost-effective purification method for $MgCl_2$-Containing salts for next-generation concentrating solar power technologies

Youyang Zhao *, Judith Vidal

National Renewable Energy Laboratory, 15013 Denver West Parkway, Golden, CO, 80401, USA

ARTICLE INFO

Keywords:
Molten chloride
Concentrating solar power
Purification
MgOHCl
Corrosion control

ABSTRACT

Next-generation concentrating solar power (CSP) technology requires a high-temperature heat-transfer fluid and thermal energy storage media. Molten $MgCl_2$-KCl-NaCl is considered a potential candidate salt due to its thermophysical properties. However, $MgCl_2$ presents various challenges because of its hygroscopic nature. To keep corrosion under control, this molten chloride needs to remain free of hydrates and other impurities. Here, we have developed an effective purification method for $MgCl_2$-containing salts by 1) combining known laboratory-scale, batch-style thermal and chemical purification processes to enable scalable, continuous-style processes for commercial next-generation CSP operation; 2) improving overall efficiency and minimizing the major corrosive impurity MgOHCl by optimizing key engineering parameters such as heating temperature/time and amount of elemental Mg addition; and 3) investigating the addition of halite (NaCl) to carnallite ($KMgCl_3$) to reduce the liquidus temperature. Laboratory-scale results suggest that 1) adding 6.5 wt% of halite and less than 0.1 wt% of elemental Mg to commercial carnallite and 2) following a heating schedule to at least 650 °C with ~3 h of holding time at that temperature can produce a ternary $MgCl_2$-KCl-NaCl salt composition with a low liquidus temperature of about 400 °C. It also reduces the presence of the corrosive impurity, MgOHCl, from ~1 to 2 wt.% to ~0.1 wt%. Findings of these key engineering parameters should provide a pathway toward a scalable, continuous-style salt-purification process at a scale of metric tons per hour that can produce a corrosion-controlled chloride molten salt for CSP applications.

1. Introduction

Next-generation (Gen3) concentrating solar power (CSP) technology requires heat-transfer fluids (HTFs) and thermal energy storage (TES) that can operate in the temperature range of 500°–720 °C [1]. The molten nitrate HTF/TES used for current-generation CSP technology can be operated only up to 565 °C. So, a new HTF/TES chemistry is required with higher thermal and chemical stabilities, comparable energy density, and low corrosion on metallic materials used in heat exchangers, piping, and TES tanks. To achieve such goals, a ternary chloride-salt system, $MgCl_2$-KCl-NaCl, has been proposed by the U.S. Department of Energy's Salt Consortium. This molten-salt system is thermally stable without decomposition beyond the highest operating temperature of the supercritical CO_2 power cycle (i.e., 720 °C). However, the corrosion properties of the ternary salt are less known. The corrosion mechanism is believed to be correlated to the presence of an impurity, magnesium hydroxychloride (MgOHCl), at the operation temperatures [2–6]. Hydroxychloride formation had also been found in other salts such as $CaCl_2$ [7–13]. This corrosive impurity is produced during hydrolysis of anhydrous salt because of the hygroscopic nature of the ternary salt's key component—$MgCl_2$; that is, when $MgCl_2$ is exposed to moist atmospheres, it can form $MgCl_2 \cdot H_2O$, $MgCl_2 \cdot 2H_2O$, $MgCl_2 \cdot 4H_2O$, and $MgCl_2 \cdot 6H_2O$. To mitigate the risks associated with the formation of these species, multiple methods for controlled salt dehydration and purification have been proposed, such as: thermal treatment by controlled heating [3,7,14–22], magnesiothermic reduction by elemental Mg [2,23–25], dehydration with ammonium chloride [3,21,26–28], and carbochlorination with CO, Cl_2, and/or CCl_4 to remove oxide species [27,29–31]. Because the targeted CSP industry needs a significant amount of salt inventory (>10,000 Mt) for each power plant, our intent is to investigate the most cost-effective and scalable salt-purification process that can be adopted by this industry.

* Corresponding author.
E-mail address: youyang.zhao@nrel.gov (Y. Zhao).

https://doi.org/10.1016/j.solmat.2020.110663
Received 14 January 2020; Received in revised form 9 June 2020; Accepted 12 June 2020
Available online 29 June 2020

Ammonium chloride dehydration and carbochlorination both need to handle hazardous and toxic gases [32]. Therefore, the present work is mostly motivated by the relative ease of thermal dehydration of $MgCl_2$ hydrates and the magnesiothermic reduction of corrosive impurities. Dehydration of hydrates (Eqs. (1a)–(1d)) and hydrolysis to form MgOHCl (Eqs. (2a) and (2b)) at specific temperature ranges are in many cases competitive and have been discussed in the literature [3,7,10,13,18,20,21,33–38].

$$MgCl_2 \cdot 6H_2O = MgCl_2 \cdot 4H_2O + 2H_2O \text{ at } 96^\circ - 117^\circ C \quad (1a)$$

$$MgCl_2 \cdot 4H_2O = MgCl_2 \cdot 2H_2O + 2H_2O \text{ at } 107^\circ - 180^\circ C \quad (1b)$$

$$MgCl_2 \cdot 2H_2O = MgCl_2 \cdot H_2O + H_2O \text{ at } 153^\circ - 242^\circ C \quad (1c)$$

$$MgCl_2 \cdot H_2O = MgCl_2 + H_2O \text{ at } 304^\circ - 400^\circ C \quad (1d)$$

$$MgCl_2 \cdot 2H_2O = MgOHCl + HCl(g) + H_2O \text{ at } 193^\circ - 240^\circ C \quad (2a)$$

$$MgCl_2 + H_2O = MgOHCl + HCl(g) \text{ at } 210^\circ - 445^\circ C \quad (2b)$$

These reactions, combined with the thermal decomposition of MgOHCl [3,19,39],

$$MgOHCl = MgO + HCl(g) \text{ at } 533^\circ - 568^\circ C, \quad (3)$$

will 1) produce a corrosive HCl/H_2O mixture, 2) irreversibly shift the overall salt composition, and 3) eventually form 1 mol of MgO for each mole of $MgCl_2$ involved, as shown below [35,37].

$$MgCl_2 + H_2O = MgO + 2HCl(g) \text{ at } 455^\circ - 468^\circ C \quad (4)$$

These reactions can be a serious issue because they can introduce corrosive HCl gas and may lead to changes in several thermophysical properties such as 1) melting (or freezing) point, which can jeopardize the safe operation of the CSP plants, and 2) heat capacity and density, which can decrease the overall power-generation capability of the CSP plants when integrated with the supercritical CO_2 Brayton power cycle. In addition, production of MgO, in the form of fine particulates, can risk clogging the small channels in the primary heat exchanger and wearing out the bushing and bearings used in the salt pumps. Therefore, proper purification of $MgCl_2$-containing chloride salt is needed.

Some efforts to understand the reversibility of the reactions above have attempted to find a means to suppress the formation of HCl and MgOHCl. Chlorination of MgOHCl with HCl or Cl_2 to form $MgCl_2$ and H_2O (e.g., the reverse reaction of Eq. (2b)) was investigated by Ref. [40,41]. However, the kinetics of chlorination gradually diminish as chlorination time increases, which seems independent of chlorination temperature; this may possibly be due to the back reaction when H_2O is generated. Similarly, the reverse reaction of Eq. (4) was also investigated between 450° and 650 °C [42]. The reaction kinetics slow down as diffusion of HCl through the layer of $MgCl_2$, the reaction product, dominates over the chemical reaction between MgO and HCl. At industrial scale, using HCl or Cl_2 requires corrosion-resistant hardware and gas-scrubbing systems for environmental, health, and safety reasons. Hence, such a method is not practical for the cost-sensitive CSP industry, where the targeted TES cost is $15/kWh-thermal as set by the U.S. Department of Energy; this overall cost includes materials cost, processing cost, and all relevant hardware cost (e.g., TES tanks).

In a recent work [6], the same authors at the National Renewable Energy Laboratory (NREL) investigated a two-step purification process for a commercial chloride salt based on a known thermal [3,7,14–22] and chemical treatment [2,23–25]. The raw salt used in Ref. [6] has a water content of about 5.5 wt%, i.e., 5 to 10 times higher than the salt used in the present work. Such high water content required a very time-consuming step-wise dehydration and purification process where the thermal treatment dehydrated the commercial salt at 117 °C for 8 h, 180 °C for 8 h, 240 °C for 2 h, 400 °C for 1 h, and 600 °C for 1 h, with a heating rate of 5 °C/min between the isothermal steps. The chemical treatment used 1.7 wt% of elemental Mg at 850 °C for 1 h to reduce MgOHCl and other cationic impurities such as Fe^{3+}. Similarly, a most recent investigation, using Raman and infrared spectra, on the corrosion behaviors of similar ternary chloride salt treated by elemental Mg [25] also confirmed the effectiveness of this metal in reducing impurities and salt's corrosivity in various Ni alloys. Evidence showed that a raw salt with much lower water content[1] may not need the full thermal treatment as described by Ref. [6], especially for the steps below 300–400 °C. Also, the 1.7 wt% addition of elemental Mg will certainly be in great excess.

Therefore, motivated by the successes and shortcomings of [6] and other literature mentioned above, the key objectives of our current work are to 1) further optimize a cost-effective purification process that is able to minimize the presence of corrosive impurities, 2) investigate a purer commercial chloride salt compared to what was used in Ref. [6] that allows us to understand real-world challenges, and 3) propose a scalable single-step purification process and provide key engineering parameters to enable an industrial continuous-style process (e.g., purification temperature/time and amount of Mg/halite addition to achieve optimal salt composition with low liquidus temperature and high purity). Our goal is to contribute a comprehensive package to the industry with these parameters and transfer our scientific findings to engineering know-how that will eventually enable the deployment of molten chlorides for CSP and other relevant molten-salt applications.

2. Experimental

Materials: Raw materials used were anhydrous carnallite (AC) from Israel Chemicals Ltd (ICL) of approximate composition $49.1MgCl_2$–38.6KCl–12.3NaCl (wt.%) with 0.5–1 wt.% of water and Silver Peak (SPK) halite from Albemarle Corporation of approximate composition 92.5NaCl–6.0KCl–$1.4CaSO_4 \cdot 2H_2O$ (wt.%). Note that there are other minor salt components provided by ICL and Albemarle (Table 1).

Purification setup: Fig. 1 gives the schematic of the purification setup showing the crucible (fused-quartz crucible, part# FQ-2500 or FQ-2800, AdValue Technology), gas sparger (alumina single-bore tube, part# AL-T-N1/4-N3/16-12, AdValue Technology), stainless-steel (SS) 304 test vessel (150-mm inner diameter, 350-mm height), SS304 gas inlet and outlet, type-K thermocouple (part# CAIN-18G-18, Omega Engineering), and nickel crucible cover (part# Z246700-1EA, Sigma Aldrich). About 500–800 g of AC was used for each purification batch, where 6.5 wt% of SPK halite and 0–0.75 wt% of elemental Mg (chips, 6–35 mesh size, 99.98% trace metals basis, part# 254118, Sigma

Table 1
Chemical analysis of AC and SPK halite provided by ICL and Albemarle, respectively. Empty cells indicate that the element or ion is not reported or detected.

	Unit	ICL AC	SPK Halite
Mg	wt.%	11.4	0.125
K		20.8	1.80
Na		4.9	23.5
Ca	ppm		3848
Br		3900	
Fe		46.2	
Mn		3.36	
Li			378
SO_4^{2-}		203	
S			3425
Zn		<1	

[1] Usually as a result of dehydration by the salt supplier.

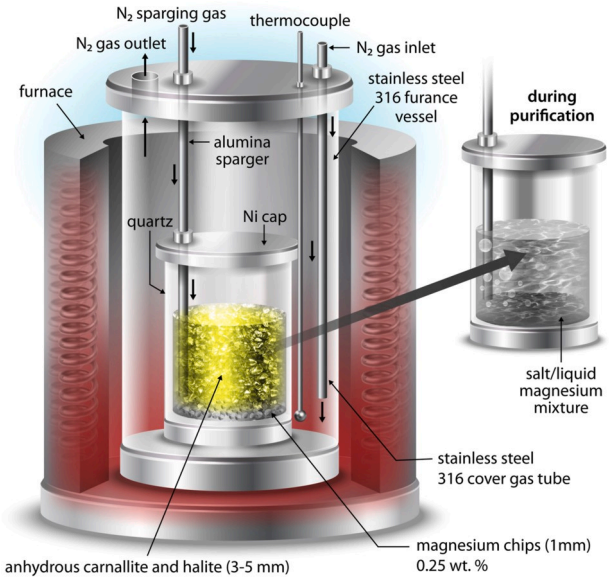

Fig. 1. Schematic showing the purification setup.

Aldrich) were added to achieve the desired salt composition and perform chemical purification, respectively. Dry nitrogen (N_2) gas (<10 ppm oxygen, <1 ppm moisture) was used as the sparging and cover gas.

Purification procedures: AC, SPK halite, and Mg chips were loaded without mixing into the fused-quartz crucible in an inert glove box (<0.5 ppm of H_2O and O_2) and quickly transferred into the test vessel in a crucible furnace (Lindberg Blue M). The sparger tube, gas inlet, and gas outlet were installed according to Fig. 1. The test vessel was sealed using a grafoil gasket. The test vessel was then pumped down to less than -0.085 MPa and refilled with N_2 at least three times. N_2 was flowed through the primary gas inlet at 500 sccm and through the sparger at 150 sccm with a vessel pressure at about ~0.0069 MPa (or 1 psi) above atmosphere pressure. The slight positive pressure was adopted as precaution to prevent H_2O and O_2 ingress. The heating schedule shown in Table 2 was used for salt purification. Three separate sets of experiments were conducted to investigate the effect of chemical purification temperature, dwell time, and amount of Mg added, respectively.

After the vessel furnace was cooled to room temperature, the test vessel was opened, and the salt was retrieved and stored in the inert glove box (H_2O and O_2 levels less than 0.5 ppm) as soon as possible to minimize exposure to moisture and oxygen in the ambient atmosphere.

pH monitoring of the outlet gas: We continuously monitored the pH change of an acetic acid aqueous buffer solution (0.1 M acetic acid and 0.1 M sodium acetate in 1 L of DI water) connected to the gas outlet of the purification furnace. The goal was to capture HCl released from purification and determine the end of HCl generation (i.e., an indication of the completion of salt purification). The stainless-steel tube connecting the furnace gas outlet to the buffer solution was heated at ~120 °C to minimize condensation of HCl and corrosion in the tube.

Table 2
Heating schedule for AC salt purification. X°C and Y h are the chemical purification temperature and dwell time, respectively, under investigation. "R.T." means room temperature.

Step	Temperature	Ramp rate	Hold time	Active N_2 sparging?
1	R.T. to 250 °C	1 °C/min	2 h	Yes
2	250 °C to X°C		Y h	
3	X°C to R.T.		No holding	Sparger is lifted out of the molten salt at the beginning of step 3

Chemical composition and MgOHCl impurity analysis: The chemical composition of the purified salt was then analyzed by inductively coupled plasma–atomic emission spectroscopy (ICP-AES). The MgOHCl content was analyzed by a titration technique developed by the authors [43]. The titration technique utilized the different solubilities of the chloride salts, MgO and MgOHCl in methanol and DI water to achieve physical separation of these components via dissolution and vacuum filtration. The amounts of the Mg-bearing species ($MgCl_2$, MgO and MgOHCl) were determined by a well-known ethylenediaminetetraacetic acid (EDTA) titration used in wastewater analysis.

3. Results and discussion

3.1. Effect of thermal and chemical purification for AC

Our goal is to optimize the salt purification process reported in Ref. [6] by eliminating certain thermal treatment steps and reducing the amount of Mg addition. So, it is important to fully understand each step's effect by measuring MgOHCl from samples taken after each step (i.e., 117 °C for 8 h, 180 °C for 4 h, 240 °C for 2 h, 400 °C for 1 h, and 600 °C for 1 h and with addition of 0.25 wt% Mg). This procedure is to establish a baseline for future comparison with optimized processes.

Fig. 2 shows the corresponding MgOHCl content at each step of the separate thermal and chemical treatments. We should clarify that the chemical treatment with 0.25 wt% of Mg was applied subsequently, after the full thermal treatment steps given in Fig. 2, instead of a standalone chemical purification on the as-received AC. During the thermal purification steps, no significant increase of MgOHCl was observed until the "400 °C for 1 h" step. The MgOHCl content subsequently decreased after treatment at 600 °C, and a much lower content was observed for the AC salt mixture thermally and chemically purified (red bar in Fig. 2). ICL claims that AC has a 0.5 wt% water content, either in the form of physically absorbed moisture or hydrate. Based on this amount, we can calculate that the average hydrate number x in $MgCl_2 \cdot xH_2O$ is less than 1 given the approximate AC composition of 49.1$MgCl_2$–38.6KCl–12.3NaCl (wt.%). This means that $MgCl_2$ is present mostly as anhydrous $MgCl_2$, with a minor amount of $MgCl_2$ hydrate—most likely $MgCl_2 \cdot H_2O$. The variation of MgOHCl content shown in Fig. 2 and the known dehydration chemistry in Eq. (1a)-(1d) corroborates this hypothesis because MgOHCl content during thermal purification does not show a major increase until 400 °C. $MgCl_2$ hydrolysis to form MgOHCl (i.e., Eqs. (2a) and (2b)) can occur at as low as ~240 °C [3,20,22,44], but there was either insufficient $MgCl_2 \cdot 2H_2O$ in the

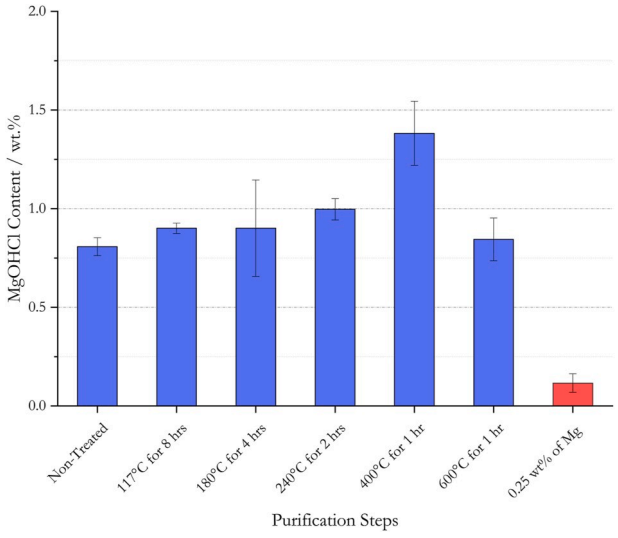

Fig. 2. MgOHCl content measured in AC salt subject to different purification treatment.

as-received AC to support Eq. (2a), or insufficient water molecules released from dehydration of a higher hydrate to support Eq. (2b) until 400 °C, where dehydration of $MgCl_2 \cdot H_2O$ can occur. Both reactions are a result of AC's low average hydrate number (i.e., <1). Therefore, we only see major MgOHCl increase after the "400 °C for 1 h" step.

In addition, we observed a significant reduction of MgOHCl at 600 °C due to thermal decomposition of MgOHCl given by Eq. (3). During chemical purification with 0.25 wt% of Mg, we observed a further reduction of MgOHCl to ~0.1 wt% according to the following reaction [2]:

$$2MgOHCl + Mg = 2MgO + MgCl_2 + H_2 \quad (5)$$

Given the significant reduction of MgOHCl content at this step, Mg chemical purification is considered the primary salt-purification mechanism. The MgOHCl variation in Fig. 2 with AC resembles the results from Ref. [6], but it shows 4- to 6-fold lower MgOHCl during each thermal and chemical purification step because of the much lower initial water content in AC. This result suggests that 1) AC is indeed a purer raw material and 2) purification optimization by eliminating and/or combining thermal treatment steps and reducing Mg addition is promising because of the lack of a higher form of $MgCl_2$ hydrates in raw AC and lower amount of MgOHCl that can be produced during purification.

Examination of MgOHCl content in the salt during the thermal purification seems to suggest that this process alone is not quite effective at reducing MgOHCl content—i.e., 0.75 wt% remains after thermal purification compared to the initial ~0.6 wt% in the non-treated raw AC. This is primarily due to the increase of MgOHCl via hydrolysis. Therefore, a key implication from Fig. 2 is that thermal purification can be more effective if hydrolysis-formed MgOHCl can be minimized by reducing the residence time of the salt at ~400 °C. Along with the confirmation that AC salt is lower in moisture and hydrate content than previous purified dehydrated carnallite (DC) in Ref. [6], it also suggests that a more energy-efficient, less time-consuming purification procedure compared to the ones shown in Fig. 2 can be carefully designed because there are minimal amounts of $MgCl_2 \cdot 6H_2O$, $MgCl_2 \cdot 4H_2O$, and $MgCl_2 \cdot 2H_2O$ in the raw AC salt compared with those in DC. So, thermal purification steps at 117 °C, 180 °C, and 240 °C are not necessary. It is also preferable, from the perspective of economics and scalability, to reduce the exposure time of the salt to the temperature window between 400 °C and the temperature at which Mg chemical purification is more effective (to be discussed). This temperature window also corresponds to significant release of HCl gas.

Previous work by the same authors [6] discovered that there is a strong correlation between MgOHCl content of the salt and corrosion rates of Haynes 230. An over ten-fold decrease of MgOHCl (i.e., from ~3 wt% to ~0.1–0.2 wt%) reduces the corrosion by more than 20 folds (i.e., from ~950 μm/year to ~40 μm/year). An ongoing corrosion study on the corrosivity of the AC salt shows similar behavior. We acknowledge that contribution of corrosion by other species such as Fe^{3+} and SO_4^{2-} cannot be completely ruled out. But the fact that either the concentrations of these species are much lower than that of MgOHCl or the relative concentration changes during purification are also smaller (see Table 4) motivates our hypothesis that managing MgOHCl content in the salt is a primary method for salt purification and corrosion control. The effects from other impurity species are secondary and can be a subject of future investigation. Therefore, the optimization of the purification process discussed in this paper is based on MgOHCl minimization.

3.2. Optimization of purification

It is costly and time-consuming to treat AC plus SPK halite with stepwise isothermal heating for long durations, followed by cooling to ambient temperature to add Mg chips, and heating up again for chemical purification, as done in the previous work [6]. For large-scale salt purification, the ideal purification design would be a single-step procedure with minimum energy cost. On the materials-cost side, elemental Mg is relatively expensive at ~$4000/Mt compared to AC at ~$700/Mt. So, efficient use of this metal is key—with excessive and unreacted Mg being undesirable. From a system-design perspective, the excess Mg can cause potential problems because its melting point is ~650 °C. Molten and dissolved Mg in the hot section of the CSP loop, at ~700 °C, can solidify/precipitate in the cold section at ~500 °C due to liquid-solid phase transition and different solubilities of solid and liquid Mg in molten chlorides [45–48]. The solid precipitation presents clogging risks in the delicate channels of the primary heat exchanger. Therefore, we evaluated a single-step thermal/chemical purification with minimum Mg addition that heats the salt mixture (AC and SPK halite) and Mg chips to 250 °C for 2 h for moisture removal and up to the Mg purification temperature for a certain time (the detailed heating schedule is provided in Table 2).

3.2.1. Effect of Mg purification temperature

Fig. 3 shows the effect of Mg purification temperature during the single-step purification of as-received AC only (no halite addition). The purification was performed for 3 h at each temperature. Three hours of purification time was selected given the study on purification time discussed in Section 3.2.3. We determined MgOHCl content with titration [43] in salt mixtures purified at three different temperatures with 0.5 wt % and 0.75 wt% of Mg addition. We later performed a determination of the most-effective dwell time. We observed a clear decrease of MgOHCl content with increasing purification temperature.

Results in Fig. 3 suggest that for Mg purification to be effective at reducing MgOHCl, 650 °C is the most desirable temperature. To exclude the possibility that kinetic barriers at 500 °C and 575 °C limited the reaction between MgOHCl and Mg (Eq. (5)), we used FactSage to calculate the Gibbs free energy of the reaction [49]. The Gibbs free energy of reaction at both temperatures was found to be around -150 kJ per mole of MgOHCl suggesting that it is a highly spontaneous reaction. The moderate temperature range of 500 °C–600 °C could provide thermal activation to help overcome the reaction's activation barrier. Therefore, it is not very likely that this reaction can be severely limited by reaction kinetics. A plausible explanation why 650 °C is more desirable lies in the solubility of Mg in the ternary molten chloride salt. Although literature information is lacking on 1) Mg solubility in chloride salt with composition close to that of the purified salt or 2) solid Mg solubility in molten chloride salt, literature exists on liquid Mg solubility in some pure or binary chloride salts. The solubility of liquid Mg is about

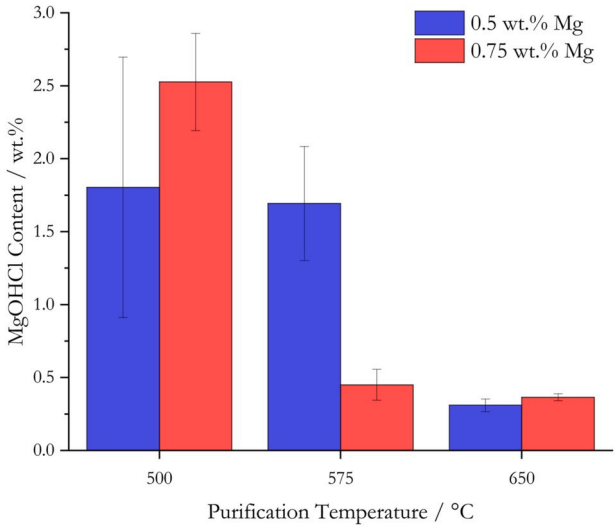

Fig. 3. MgOHCl content determined by titration as a function of purification temperature for 0.5 wt% (blue) and 0.75 wt% (red) of Mg addition to the AC. The purification time was 3 h. (For interpretation of the references to color in this figure legend, the reader is referred to the Web version of this article.)

0.1–0.5 mol% and generally increases with temperature and with decreasing amount of alkali chlorides [45–48,50,51]. Without sufficient literature support or experimental evidence, we could only speculate on a low solubility of Mg, especially when it is not molten. The lower Mg solubility may have caused the lower efficiency of MgOHCl reduction seen at lower temperatures of 500 °C and 575 °C. Another possible reason that molten Mg seems better at reducing MgOHCl is that MgO, one of the reaction products shown in Eq. (5), can potentially passivate the solid Mg surface. Post-experiment inspection showed that the remaining Mg chips after purification experiments at temperatures lower than 650 °C did exhibit a black surface layer. When dissolved in deionized water, these remaining Mg chips with the black surface clearly showed a much slower reaction with water releasing gas bubbles (i.e., H_2), compared to native Mg chips. On the contrary, MgO formation on molten Mg may be more easily broken off because of the turbulence created by inert gas sparging and the flexible/flowing nature of liquids. However, caution must be taken when interpreting these hypotheses before confirming the chemical makeup of the surface layer and whether MgO can indeed passivate the reaction in Eq. (5). In addition, we hypothesize that not all soluble MgOHCl (e.g., at 0.02 mol/kg [52] in similar molten chlorides) can equally access Mg, whether soluble or insoluble. It should be noted that the scatter of data at 500 °C and 575 °C is much larger than that at 650°C—which seems to support the aforementioned hypotheses that attempt to explain the observed inconsistency of the Mg purification power below its melting point.

To be rigorous, we acknowledge that the results in Fig. 3 do not completely exclude the possibility of using solid Mg as primary purification species because solid Mg does have a finite solubility. The reaction kinetics are fast (as suggested by Ding et al. [53] using cyclic voltammetry and inferred by the large negative Gibb's free energy of reaction), so the foreseen downside of using solid Mg (i.e., below 650 °C) is simply a longer purification dwell time. However, the objective of our work is to find a cost-effective, commercially scalable thermochemical process in terms of purification effectiveness. We chose 650 °C (or slightly above 650 °C to mitigate potential inhomogeneous temperature distribution inside the molten salt) as a practical compromise and did not further investigate purification at other temperatures given that: 1) Mg solubility increases with temperature, which should improve the reaction rate of Eq. (5); 2) higher temperature should increase the reaction rate of Eq. (3); but 3) the salt vapor pressure increases exponentially with temperature (ongoing work [54]), which can lead to excessive salt evaporation and deposition and eventual clogging of the experimental purification apparatus or even future real-scale purification tank components.

3.2.2. *Effect of amount of Mg addition*

Fig. 4 shows the effect of Mg addition (0–0.75 wt%) during the single-step purification of as-received AC (no halite addition). The purification was performed for 3 h with each Mg addition amount. Three hours of purification time was selected given the study on purification time discussed in Section 3.2.3. All experiments with Mg addition (0.25–0.75 wt%) showed signs of excess Mg droplets at the bottom of the salt sample by visual post-purification inspection. Similar behavior had been observed in Ref. [6]. Therefore, 0.25 wt% is the least amount of Mg under investigation that provides the best balance between effective reduction of MgOHCl and minimum excess of Mg after purification. To confirm this experimentally observed value, we give an order-of-magnitude calculation below based on H_2O and MgOHCl content to estimate the maximum amount of Mg needed:

1. The initial MgOHCl content in non-treated AC is on the order of 0.75 wt% (as shown by the first bar in Fig. 3), which equals 0.00977 mol of MgOHCl per 100 g of AC.
2. The H_2O content (including both physical moisture and chemical hydrates) in non-treated AC is around 0.5 wt% (according to the salt specification provided by ICL), which equals 0.0278 mol of H_2O per 100 g of AC. Assuming 100% of H_2O is used for the hydrolysis of $MgCl_2$, an additional 0.0278 mol of MgOHCl will be formed given the stoichiometry in Eq. (2b).
3. Therefore, the maximum MgOHCl that can occur in the entire course of purification is 0.00977 + 0.0278 = 0.0376 mol per 100 g of AC. This amount assumes that thermal purification does not reduce the amount of MgOHCl.
4. Based on Eq. (5), each mole of MgOHCl consumes 0.5 mol of Mg for complete reduction. Therefore, the amount of Mg needed is (0.00977 mol + 0.0278 mol) ÷ 2 × 24.305 g/mol = 0.457 g per 100 g of AC, or 0.457 wt%.

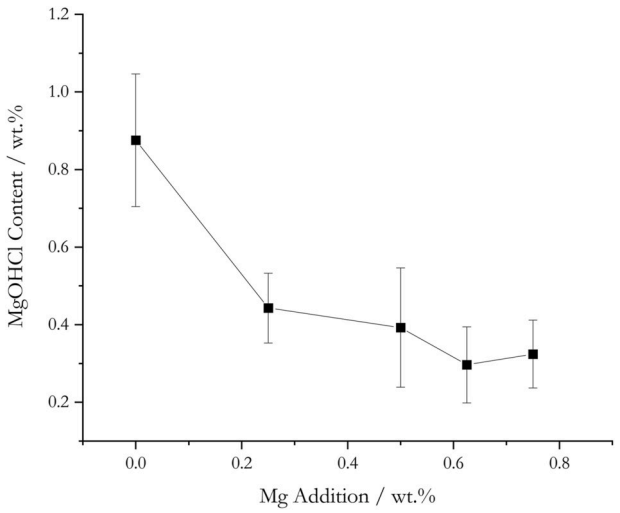

Fig. 4. The effect of Mg addition on MgOHCl content measured after salt purification at 650 °C for 3 h.

The actual amount of Mg needed for purification should be lower for the following reasons:

1. The assumption in #2 above is not accurate because 1) physical moisture can be removed at the isothermal step at 250 °C, and 2) not all H_2O released from dehydration of $MgCl_2$ hydrates can react with $MgCl_2$ to form MgOHCl at 100% efficiency.
2. The assumption in #3 above is not accurate because thermal purification does show the ability to reduce MgOHCl content (e.g., by ~50% if an isothermal step at 600 °C for 1 h is used).

Therefore, if we assume that 1) 50% of the initial water content is physical moisture (which roughly agrees with ICL's data of 0.5 wt% mass loss upon drying), 2) H_2O released from hydrates reacts with anhydrous $MgCl_2$ with 50% efficiency, and 3) thermal decomposition can reduce 50% of MgOHCl produced, then a more realistic estimation of Mg needed is (0.00977 mol + 0.0278 mol × 50% × 50 %) × 50 % ÷ 2 × 24.305 g/mol = 0.102 g per 100 g of AC, or 0.102 wt%. Our experimental observation of excess Mg after purification using 0.25 wt% of Mg also corroborates this calculation, which suggests that the most efficient amount of Mg needed should be less than 0.25 wt%. Ideally, the excess Mg remaining in the salt after purification should be quantified to provide the exact consumption of Mg. However, the separation of excess Mg from the chloride salt presents a technical challenge—namely, manual collection of solid Mg droplets is time-consuming and unreliable, and dissolution of chloride salts is not feasible because the solvents that dissolve chloride salts usually react with Mg.

Although the exact amount of Mg needed for salt purification could not be precisely quantified at lab-scale, the approximate range of 0.1–0.25 wt% should serve as a practical upper bound for future large-scale purification experiments if moisture content in the raw salt material is at a similar level of AC (e.g., 0.5 wt% H_2O). Concerns about

larger variation of industrial salt quality can be addressed first by performing similar order-of-magnitude estimations shown above to establish an upper bound of needed Mg. A MgOHCl sensor that can directly and quickly measure the MgOHCl content in the molten salt could provide feedback and then control the feed rate of raw materials and/or the residence time of the salt in the continuous purification reactors, i.e., effectively adjusting the Mg amount. In addition, the effectiveness of purification may be affected by the level of agitation in the molten salt, which can depend greatly on the specific design of a purification reactor. For these reasons, we selected 0.1 wt% of Mg addition[2] and conducted no further optimization of Mg addition. Note that purification with Mg or MgOHCl thermal decomposition (whose kinetics increase with temperature [19]) can both reduce final MgOHCl concentration. However, there is a practical trade-off between these two mechanisms when designing a large-scale process using commercial salt with different water content. When initial water (and hence, MgOHCl) content in the raw salt material is high (such as the dehydrated carnallite salt used in Ref. [6]), then having the MgOHCl thermal decomposition as the only mechanism to reduce MgOHCl is not ideal because it produces a significant amount of corrosive HCl gas that can damage the hardware. MgOHCl purification with Mg must be used to reduce the formation of HCl. When initial water content is low (such as the AC salt used in this work), then MgOHCl thermal decomposition might be sufficient to reduce this small amount of MgOHCl without producing a significant amount of HCl gas. In this scenario, a very small amount of Mg at < 0.1 wt% (or even no Mg) can be used, as suggested by recent ongoing work by the authors. Note that there is a potential disadvantage of using excessive Mg during purification. Chemical reaction of Mg with MgOHCl, HCl and/or H_2O will all generate H_2 gas with a stoichiometric ratio of 1:1. An industrial scale salt melter/purifier will most likely have a liner made of materials more resistant to HCl gas corrosion (i.e., ceramic-based refractory bricks for the melter chamber and fiber-glass composite for the off-gas pipelines). And the industry is more concerned with H_2 generation which may lead to explosion if the H_2 gas is not properly treated/diluted. Therefore, the material selection and safety concern further justify our recommendation that only small amount (e.g., 0.05 wt% or 500 ppm) of Mg is needed during purification to 1) further reduce MgOHCl in addition to MgOHCl's thermal decomposition, 2) remove other impurities such as Fe and Ni cations,[3] and 3) keep a low level of dissolved Mg[4] for continued corrosion potential control [23,24].

3.2.3. *Effect of purification time with Mg*

Fig. 5 shows the pH change of the acetic acid aqueous buffer solution connected to the gas outlet of the furnace vessel during the single-step purification of as-received AC (no halite addition) by 0.25 wt% of Mg at 668 °C. The purification temperature was slightly higher than 650 °C in this experiment to account for any temperature inhomogeneity in the salt. As indicated by the dashed vertical lines, the pH drop started at around 410 °C with pH ~4.4 and plateaued to pH ~4.1 in around 170 min. The onset temperature of 410 °C roughly agrees with the theoretical prediction of the dehydration temperature of $MgCl_2 \cdot H_2O$ where

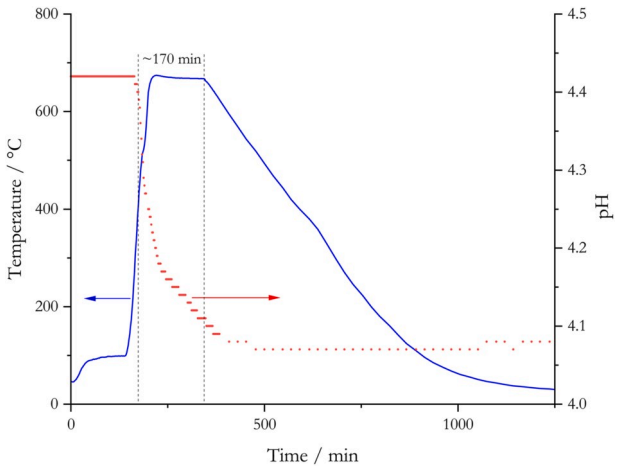

Fig. 5. Variation of pH in the buffer solution (red) and salt temperature (blue) as a function of purification time during thermal purification of 350 g of as-received AC at 668 °C. The dashed vertical lines indicate the start and finish of the pH drop. The start of pH drop is around 410 °C. Note: the "discontinuous" behavior of the pH data was due to the resolution of the pH probe at 0.01 and the data acquisition interval of 2 min. (For interpretation of the references to color in this figure legend, the reader is referred to the Web version of this article.)

released H_2O can participate in the hydrolysis reaction with anhydrous $MgCl_2$ to form HCl (as discussed previously).

The plateau of pH in Fig. 5 indicates the completion of HCl release. A theoretical calculation[5] shows that a pH drop from ~4.42 to ~4.08 in the buffer solution corresponds to HCl production of roughly 1.04 g, or 0.30 g of HCl per 100 g of AC. However, not all HCl formed had been captured by the acetic acid buffer because of potential reaction with the test hardware or excess Mg. In addition, pH monitoring has its own limitation (discussed below); hence this value should only serve as a lower bound for HCl generation. On the other hand, calculation shows that a maximum amount of 0.0556 mol, or 2.03 g, of HCl can be formed per 100 g of AC salt based on the initial content of physical moisture and chemical hydrates provided by ICL (0.5 wt%) and using the stoichiometry of hydrolysis and thermal decomposition combined (i.e., Eq. (4) indicates that each mole of H_2O can form, at maximum, 2 mol of HCl). Clearly, this amount is an upper bound because 1) the physically absorbed moisture[6] is less relevant to HCl formation because it can be removed relatively easily at ~100 °C without contributing to HCl formation, and 2) not all H_2O released will be converted to HCl because some H_2O will escape without reacting with $MgCl_2$. Therefore, if we exclude the contribution from physically absorbed moisture (0.2 wt%) and assume that 50% of released chemical hydrate participates in hydrolysis, then HCl formation will drop to 0.608 g per 100 g of AC (still higher than measured value of 0.30 g per 100 g of AC), which suggests that either the participation rate of released water is even lower than 50% or the HCl production by MgOHCl thermal decomposition is lower because MgOHCl is reduced by Mg to produce H_2 instead of HCl.

Note that the HCl calculation based on pH changes of the buffer solution is very sensitive to the accuracy of the pH measurement, especially the initial pH of the buffer (i.e., around 4.76 given the recipe in the Experimental section). However, our pH measurement was never

[2] Multiple experiments at 500 g scale with 0.1 wt% of Mg addition showed excess Mg droplets after purification, suggesting that even 0.1 wt% could serve as a practical upper bound.

[3] To remove 100 ppm of Fe, less than 70 ppm of Mg is needed assuming a reaction of $2Fe^{3+}+3Mg = 3Mg^{2+}+2Fe$.

[4] Mg solubility in the molten chloride composition investigated by this work at 650°-700 °C is estimated to be about 500–1000 ppm [46,48,50].

[5] In principle, the calculation uses the Ka value of acetic acid, initial concentrations of acetic acid and acetate ions (from sodium acetate trihydrate), and the starting and ending pH values to solve the starting and ending concentrations of H^+ ions. The difference is due to the introduction of HCl, a strong acid, generated from the purification process.

[6] Drying of AC at 110 °C revealed a mass decrease (physical moisture) of around 0.2–0.5 wt%.

able to provide an initial pH around 4.76 even after careful solution preparation and pH probe calibration with standards. Hence, we only intended to use the pH monitoring to track HCl release, which is exactly the purpose of this section of determining Mg purification time based on HCl release, instead of providing accurate quantification of released HCl.

3.2.4. Optimized salt purification procedure

The finalized optimal salt purification is summarized in Table 3, which should serve as a guideline for lab-scale purification. Note that the slow cooling at 1 °C/min without active gas sparging (Step 3) is intended to settle MgO particles that are generated due to reduction of MgOHCl via either MgOHCl thermal decomposition or reaction with Mg. Calculation based on Stokes' Law of settling revealed that less than 1 h is needed for MgO particles at 10–20 μm[7] to settle ~10 cm (i.e., the maximum height of the liquid salt). Our measurement[8] of the bottom "sludge" phase of the purified salt (which occupies about 3–5 vol% of the solidified salt) showed > 30 wt% of particles while the same measurement in the upper clean salt phase showed < 0.05 wt% of particles which suggests that we achieved very effective settling following the guideline of slow cooling and no gas sparging to avoid disturbing the settling process. Effective settling will help remove MgO particles that may cause wear damage and clogging of the mechanical subcomponents in the salt loop such as the salt pumps.

NREL and research partners verified the effectiveness of this process up to 8 kg. NREL is also collaborating with industrial partners to design a real-scale, continuous-style purification reactor using the information provided by the guideline to process salt at 1 Mt/h.

3.3. Outcome of optimized salt purification

3.3.1. Salt appearance

Fig. 6 shows the appearance of as-received AC and post-purification AC + halite. The purified salt (left) was white with roughly 3–5 vol% of dark sludge formation at the bottom, compared to the light yellow color of the as-received AC (right). The dark sludge is not shown, but it is similar to that reported by Ref. [6]. The color change was determined experimentally to be correlated to the dehydration of absorbed water and possibly a minor release of HCl at below 300 °C because water absorption could have occurred during shipment and storage of raw AC

Table 3
Finalized purification parameters at lab-scale for 0.5–1 kg of salt. "R.T." means room temperature.

6.5 g of SPK Halite and ~0.05 g of Mg per 100 g of ICL AC				
Step	Furnace temperature	Ramp rate	Hold time	Gas flow rate
1	R.T. to 250 °C	1 °C/min	2 h	150 sccm for sparging gas >500 sccm for cover gas
2	250 °C–670 °C[a]		3 h	
3	670 °C[a] to R.T.		No holding	No active sparging >500 sccm for cover gas

[a] 670 °C is recommended instead of 650 °C to provide a 20 °C margin to account for temperature inhomogeneity of the furnace equipment. Different margins can be used depending on furnace conditions.

[7] 10–20 μm is around the peak of the particle size distribution of the MgO particles as measured by a laser-based particle size analyzer.

[8] The samples were prepared by 1) dissolution in DI water, 2) vacuum filtration through 450 nm filter paper multiple times, 3) centrifugation and collection of solid particles, and 4) vacuum drying overnight to remove remaining DI water.

Fig. 6. Salt color for purified AC + halite (left) and as-received AC (right). (For interpretation of the references to color in this figure legend, the reader is referred to the Web version of this article.)

in ambient atmosphere. Thermal gravimetric analysis (TGA) with ~15 mg of a single salt grain revealed ~2–3 wt.% mass loss below 150 °C and no more major mass loss until 400 °C. After larger-scale drying of ~500 g of raw AC when heated up from room temperature to 285 °C at 5 °C/min and holding at 285 °C until water release stops (measured by a moisture sensor[9] in the off-gas), we found that the salt turned from yellow (as shown on the right in Fig. 6) to slightly off-white. The subsequent melting in the purification process then gave the salt a crystalline white appearance (as shown on the left in Fig. 6). It was not a primary goal to confirm either the hypothesis behind the color change or the exact chemistry of this intermediate species during the purification process. Rather, this was a simple experimental observation.

3.3.2. Elemental chemical analysis of pre- and post-purification salts

Table 4 shows the pre- and post-purification chemical composition of the salt measured by ICP-AES based on measurements of three as-received AC samples and four purified AC + halite samples. In both

Table 4
ICP-AES analysis of pre-purification AC salt and post-purification AC + halite salt. A total of 35 cations were analyzed. Only detectable cations were reported below. "BDL" indicates that the measurement was below detection limit.

Element	Pre-Purification AC Salt		Post-Purification AC + Halite Salt	
	Average	Stdev	Average	Stdev
	ppm			
As	34.5	3.6		BDL
Ba	1.0	0.9	1.0	0.2
Ca	905.0	90.2	1011.3	59.8
Fe	84.9	24.7	7.4	3.1
K	193,000.0	7462.6	176,108.0	8394.3
Mg	119,600.0	3736.3	102,474.0	3718.8
Mn	5.4	0.8	2.3	0.2
Mo	5.0	0.6	4.0	0.8
Na	46,033.3	2867.6	50,770.8	3394.1
P	381.3	48.1	265.4	30.4
S[a]	149.2	13.4	55.7	20.1
Sr	20.3	4.1	21.8	2.4
Zn	9.3	2.6	5.3	0.3
Co	2.3	N/A	2.8	0.5

[a] The existing form of S is SO_4^{2-} according to the chemical analysis provided by the salt suppliers.

[9] Water level was 200,000–300,000 ppm in our experiments at its peak value. We used similar flow rates of sparging gas and cover gas specified in Table 3.

pre- and post-purification salts, Mg, K, and Na are the dominating species, followed by Ca at around 900–1000 ppm, P at 250–400 ppm, and S at 50–150 ppm. All other cations were mostly below 10 ppm. Note that there is a general trend of larger stdev-to-average ratio in lower concentration elements. Such behavior is consistent in both pre-purification salt and post-purification salt. Therefore, we believe this statistical scatter is intrinsic to the ICP-AES. The intent of showing the ICP-AES results is to confirm that the elemental makeup of the purified salt is within expected limits; i.e., there is no significant loss of the major salt components (Mg, K, and Na) and no significant increase of other species due to potential contamination during purification.

Several observations are summarized below:

- There is major reduction of Fe (from ~85 ppm to < 10 ppm) and As (from ~35 ppm to below detection limit). The Ca concentration increases slightly from ~900 ppm to above 1000 ppm.
- P and S slightly decrease from ~380 ppm to ~260 ppm and from ~150 ppm to ~50 ppm, respectively.
- Other minor species (e.g., As, Ba, Mn, Mo, Sr, Zn, and Co) at much lower ppm levels are not considered here.

These changes of elemental composition can possibly be explained with known thermodynamics in the chloride system. The chloride Ellingham diagram [6,55] shows that Fe and As cations are less stable than Mg cations in the chloride system whereas Ca cations are more stable. Therefore, the reduction of Fe and As after Mg purification qualitatively agrees with thermodynamic prediction. Although Ca is expected to remain constant, the slight increase of Ca is most likely due to more Ca introduced from SPK halite because SPK halite has >3800 ppm of Ca. The P and S concentrations in the salt cannot be readily predicted by the chloride Ellingham diagram because they are likely present in the form of a sulfate (SO_4^{2-}) or phosphate (PO_4^{3-}) instead of chloride, which could be confirmed by ion chromatography in future studies. In addition, we cannot completely rule out the possibility that other unknown chemical reactions could have occurred. Therefore, caution needs to be taken when relying on the thermodynamic reduction potential series or Ellingham diagram as the sole explanation for the changes in elemental compositions. Given the relatively low concentrations of the minor species that should have limited effects on the thermophysical properties of the salt, we did not intend to identify the exact cause of their concentration changes.

3.3.3. Final salt composition

The final MgOHCl content in the purified AC + halite salt following the purification procedures was measured to be 0.11 ± 0.02 wt% based on more than 15 samples from more than 10 purification batches. Table 5 shows the calculated chemical composition of the purified AC + halite salt based on four batches given the elemental chemical analysis by ICP-AES (Table 4). The ICP-AES sample was prepared after methanol filtration that separates the chlorides from MgO and MgOHCl as described by Ref. [43] to avoid errors from these species.

Fig. 7 shows the liquidus projection of $MgCl_2$-KCl-NaCl predicted by FactSage and its database [49], where the colored isotherms correspond to the liquidus temperatures (calculated between 380 °C and 500 °C). The compositions of the raw materials (AC from ICL and SPK halite from Albemarle) are marked by blue dots, and the composition of the purified salt (Table 5) is marked by the red dot. The radius of the red dot corresponds to ~1.85 wt% (i.e., the highest standard deviation of $MgCl_2$, KCl, and NaCl reported in Table 5) to show the possible compositional variation of the purification process and its relative size compared to the region where all salt compositions remain liquid at 500 °C (i.e., the entire area enclosed by the isotherm of 500 °C). We are particularly interested in 500 °C because it is taken as the lower bound of the operating temperature for the supercritical CO_2 Brayton power cycle to be deployed for Gen3 CSP.

Table 5
Average composition and standard deviation (Stdev) of purified chloride salt following the purification procedures described in the Experimental section. The composition was calculated based on ICP-AES measurements of four purifications. The salt was prepared after methanol filtration to separate chlorides from MgO and MgOHCl.

Composition	$MgCl_2$	KCl	NaCl
		wt.%	
Average	45.98	38.91	15.11
Stdev	1.71	1.85	1.01

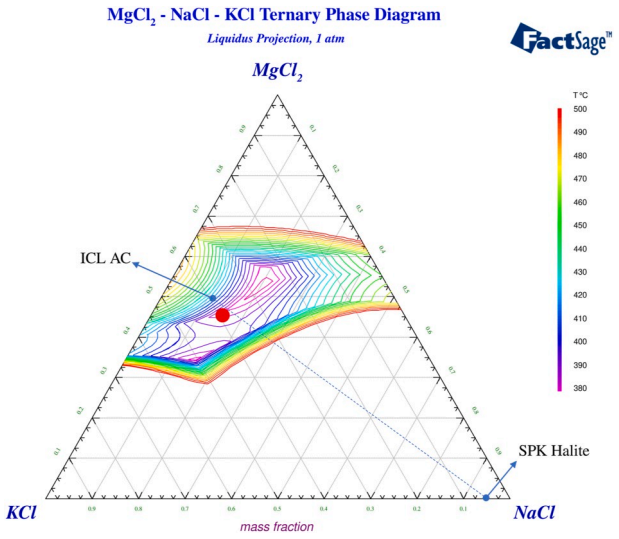

Fig. 7. Diagram of liquidus projection of NaCl-KCl-$MgCl_2$ calculated by FactSage. Blue dots: salt compositions of raw materials – AC from ICL and SPK halite from Albemarle. Red dot: salt compositions of purified salt. The radius of the red dot corresponds to the highest standard deviation of $MgCl_2$, KCl, and NaCl reported in Table 5. The blue dashed line helps to visualize the compositions that can be achieved by mixing ICL AC and SPK halite. (For interpretation of the references to color in this figure legend, the reader is referred to the Web version of this article.)

The red dot is slightly off the dashed line where the composition of any simple mixture of ICL AC and SPK halite is supposed to be located. The shifting in composition is attributed to MgOHCl thermal decomposition (Eq. (3)) and the purification process with Mg (Eq. (5))—i.e., two coexistent mechanisms that reduce MgOHCl. Eqs. (1)–(3) show that, assuming MgOHCl thermal decomposition is the sole mechanism, for each mole of MgOHCl generated from $MgCl_2$ hydrolysis and later eliminated by thermal decomposition, then 1 mol of $MgCl_2$ will be permanently lost to MgO.

On the other hand, if assuming purification with Mg is the sole mechanism, then only a half mole of $MgCl_2$ will be lost for each mole of MgOHCl eliminated (e.g., by combining Eqs. (2b) and (5)). Therefore, a composition shift away from the $MgCl_2$ corner in Fig. 7 should be expected. The exact composition shift depends on the extent of each mechanism, which cannot be easily quantified. An order-of-magnitude calculation (i.e., similar to that used for estimating ideal Mg addition shown in the "Effect of Amount of Mg Addition" section) shows that the magnitude of composition shift in $MgCl_2$ can be 0.40–1.79 wt%. The composition of the salt mixture following the recipe given in the Experimental section (i.e., 6.5 g of SPK halite per 100 g of AC), assuming no composition shift, is calculated to be 46.1$MgCl_2$–36.6KCl–17.2NaCl (wt.%). A shift of 0.40–1.79 wt% of $MgCl_2$ is able to move this composition in the range indicated by the red dot. Note that a potential, unmatched composition shift of KCl and NaCl can potentially be explained by the following.

1. There is an inherent composition variation of the raw materials. For example, the AC salt composition reported by the supplier on the specific salt batch used by our work has a NaCl content almost 3 standard deviations (i.e., 1.29 wt%) away from the yearly average value measured on a monthly basis. The difference is 1.5 standard deviations (i.e., 0.95 wt%) for $MgCl_2$ content.
2. The discrepancy between AC compositions reported by the supplier and measured by our present work is also on the order of 1–2 wt.%, suggesting that the measurement techniques used were not consistent either.
3. Similar discrepancy in compositions is also found in the SPK halite.

Therefore, it is very challenging to analyze and pinpoint the exact cause of the unmatched composition given the uncertainty of the true salt compositions. However, unpublished, ongoing work on the thermophysical properties of the purified salt suggests that thermophysical properties such as density, viscosity, and heat capacity are not sensitive to composition variations that are similar in magnitude to the compositional uncertainty. So, practically, it is not a top priority for our present work to resolve the issues of the unmatched KCl and NaCl content as long as these contents fall into the range specified by the red dot in Fig. 7. The higher priority is to confirm that the proposed purification process can reduce MgOHCl from the perspective of corrosion control, as demonstrated by the aforementioned experimental efforts.

3.3.4. Effect of halite addition

The liquidus temperature of the ICL AC is around 450°–470 °C as reported by ICL whereas the lowest liquidus temperature (i.e., eutectic temperature) in the $MgCl_2$-KCl-NaCl ternary system is 385 °C ± 1 °C [56]. Hence, the major objectives of adding SPK halite is to 1) lower the liquidus temperature of the ICL AC and provide an extra safety margin for CSP loop operation between 500 °C and 720 °C, and 2) reduce overall cost of the salt inventory because SPK halite is significantly cheaper than ICL AC by more than an order of magnitude. Therefore, we confirmed the halite's effect of liquidus-temperature reduction by performing differential scanning calorimetry (DSC) on the purified AC (following the purification process given in the Experimental section but without halite addition) and purified AC with halite addition.

The isotherms in Fig. 7 show that the liquidus temperature of the purified salt composition (red dot) is around 400 °C. Our DSC measurements of the purified AC at 20 °C/min heating and cooling rate[10] without and with the prescribed 6.5 wt% of SPK halite (Fig. 8) revealed that the addition indeed effectively decreased the liquidus temperature. The heating traces (the curves with negative DSC signal) of both samples show an onset of melting at ~400 °C (or the pseudo-eutectic temperature of the pseudo-binary system between AC and halite), which means that their compositions are on the same pseudo-binary system. The onset of 400 °C also semiquantitatively confirms that the composition of the purified AC + halite is indeed close to the composition range measured by ICP-AES (i.e., the red dot in Fig. 7). The heating trace for AC exhibits a subtle minor secondary peak (or a broad hump) on the order of -0.3 μV/mg below the baseline signal (roughly -0.15 μV/mg) around 425°–450 °C, which suggests that the composition of purified AC without halite has an off-eutectic behavior. Because no secondary peak is observed for AC + halite, it suggests that the mixture is very close to the pseudo-eutectic composition in the AC-halite pseudo-binary system.

Inspection of the cooling traces (the curves with positive DSC signal) more clearly demonstrate the pseudo-eutectic behavior of AC + halite (i.e., only one phase-transformation during solidification) vs. the off-eutectic behavior of AC (i.e., at least two major phase-transformations during solidification). It also reveals that the temperature at which the AC + halite starts to solidify is around 380 °C. It is lower than the pseudo-eutectic temperature due to liquid undercooling behavior, which is common in molten-salt systems. This solidification temperature is a critical design parameter for CSP because HTF solidification at temperatures close to the outlet of the primary heat exchanger (e.g., ~500 °C) risks damaging several CSP components. One major objective of the salt-composition optimization is to reduce the solidification of the ternary chloride salt to at least below 450 °C, giving a 50 °C safety margin because the lowest temperature of the primary heat exchanger for the supercritical CO_2 power cycle is around 500 °C.

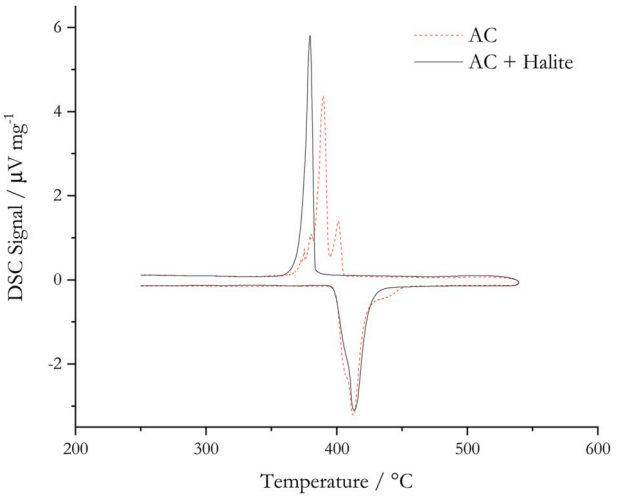

Fig. 8. DSC heating and cooling traces for purified AC and purified AC with SPK halite (6.5 g of halite added to each 100 g of AC). Heating and cooling are both at 20 °C/min.

Therefore, our DSC measurements lead to an important conclusion: the addition of SPK halite following our recipe is effective at producing the optimal salt composition with a pseudo-eutectic behavior with a low solidification temperature of ~380 °C, 20 °C lower than the melting point most likely due to the undercooling effect of the solidifying liquid. Even without any undercooling effect, solidification of the purified salt should not exceed the true melting point of 400 °C.

4. Conclusion

An optimized salt-purification process based on a combined thermal and chemical treatments was developed at NREL and allowed consistent purification of a low-cost, commercial $MgCl_2$-KCl-NaCl chloride salt. This salt is selected as the HTF and TES medium for Gen3 molten salt CSP testing at a pilot-unit scale due to its balance between cost and purity (i.e., low water content). The lab-scale purification process was 1) demonstrated to be effective at reducing corrosive species, such as MgOHCl, 2) optimized with a focus on reducing the amount of purification steps and time, thermal energy, and relatively expensive purifying-agent material, and 3) shown to produce an optimal salt composition with solidification temperature less than 400 °C which is compatible with the super-critical CO_2 Brayton power cycle. A key finding is that a very small amount of Mg at hundreds of ppm (or no Mg) is needed as purification agent for this raw salt with low level of initial water content (~0.5 wt%). This is a compromise between the purification kinetics and practical concerns with hydrogen generation and its potential flammability at high temperature. For raw salt materials with higher water content, it will be the focus of future studies to inform the relationship between the initial water content and the amount of Mg needed.

In summary, our work provided several basic parameters for effective purification of commercial $MgCl_2$-KCl-NaCl chloride salt (e.g.,

[10] DSC measurements on AC alone at 5 °C/min and 10 °C/min were also performed to investigate potential effects from slower heating. The results were largely similar where the peak splitting between the eutectic and liquidus peaks was only marginally improved.

purification temperature, time, amount of Mg needed). Although the work is at lab-scale with a simplified scenario using a batch-style process, it demonstrates the first required steps toward future and feasible scaling-up to a real commercial-scale continuous design capable of producing >10,000 Mt of $MgCl_2$-containing salts. NREL is currently involved in another project working with industrial partners who are using the optimized purification procedure to design a continuous-style purification reactor to process AC salt at 1 Mt/h, where complicated mass- and heat-transfer effects will be addressed.

Data availability

The raw and processed data required to reproduce these findings are available to download from https://doi.org/10.17632/79s6fbg67s.1.

Declaration of competing interest

The authors declare that they have no known competing financial interests or personal relationships that could have appeared to influence the work reported in this paper.

CRediT authorship contribution statement

Youyang Zhao: Conceptualization, Methodology, Investigation, Formal analysis, Writing - original draft, Writing - review & editing, Supervision, Project administration. **Judith Vidal:** Conceptualization, Methodology, Writing - review & editing, Supervision, Project administration, Funding acquisition.

Acknowledgement

This work was authored by the National Renewable Energy Laboratory, operated by Alliance for Sustainable Energy, LLC, for the U.S. Department of Energy (DOE) under Contract No. DE-AC36-08GO28308. This material is based upon work supported by the U.S. Department of Energy's Office of Energy Efficiency and Renewable Energy (EERE) under the Solar Energy Technologies Office Award Number DE-EE00033870. Additional funding was provided by U.S. Department of Energy's Office of Science and Office of Workforce Development for Teachers and Scientists (WDTS) under the Community College Internship (CCI) program and the Science Undergraduate Laboratory Internship (SULI) program. The views expressed in the article do not necessarily represent the views of the DOE or the U.S. Government. The U.S. Government retains and the publisher, by accepting the article for publication, acknowledges that the U.S. Government retains a nonexclusive, paid-up, irrevocable, worldwide license to publish or reproduce the published form of this work, or allow others to do so, for U.S. Government purposes. The authors gratefully acknowledge Mr. Jakob Chandler and Mr. Zack Krajnak for their contributions.

Appendix A. Supplementary data

Supplementary data to this article can be found online at https://doi.org/10.1016/j.solmat.2020.110663.

References

[1] M. Mehos, C. Turchi, J. Vidal, M. Wagner, Z. Ma, C. Ho, W. Kolb, C. Andraka, A. Kruizenga, Concentrating solar sower Gen3 demonstration roadmap, NREL, 2017.
[2] W. Ding, A. Bonk, J. Gussone, T. Bauer, Electrochemical measurement of corrosive impurities in molten chlorides for thermal energy storage, J. Energy Storage 15 (2018) 408–414.
[3] G.J. Kipouros, D.R. Sadoway, A thermochemical analysis of the production of anhydrous $MgCl_2$, J. Light Met. 1 (2001) 111–117.
[4] D.F. Williams, Assessment of candidate molten salt coolants for the advanced NGNP/NHI heat-transfer loop, Oak Ridge, Tennessee, 2006.
[5] D.L. Maricle, D.N. Hume, A new method for preparing hydroxide-free alkali chloride melts, J. Electrochem. Soc. 107 (2007) 354.
[6] Y. Zhao, N. Klammer, J. Vidal, Purification strategy and effect of impurities on corrosivity of dehydrated carnallite for thermal solar applications, RSC Adv. 9 (2019) 41664–41671, https://doi.org/10.1039/C9RA09352D.
[7] H.U. Rammelberg, T. Schmidt, W. Ruck, Hydration and dehydration of salt hydrates and hydroxides for thermal energy storage - kinetics and energy release, Energy Procedia 30 (2012) 362–369.
[8] H. Kondo, Z. Asaki, Y. Kondo, Hydrolysis of fused calcium chloride at high temperature, Metall. Trans. B. 9B (1978) 477–483.
[9] K.M. Allal, J.C. Dolignier, G. Martin, Determination of thermodynamical data of calcium hydroxychloride, Oil Gas Sci. Technol. 52 (1997) 361–368, https://doi.org/10.2516/ogst:1997046.
[10] A.D. Pathak, I. Tranca, S.V. Nedea, H.A. Zondag, C.C.M. Rindt, D.M.J. Smeulders, First-Principles study of chemical mixtures of $CaCl_2$ and $MgCl_2$ hydrates for optimized seasonal heat storage, J. Phys. Chem. C 121 (2017) 20576–20590, https://doi.org/10.1021/acs.jpcc.7b05245.
[11] K.S.P. Karunadasa, C.H. Manoratne, H.M.T.G.A. Pitawala, R.M.G. Rajapakse, Relative stability of hydrated/anhydrous products of calcium chloride during complete dehydration as examined by high-temperature X-ray powder diffraction, J. Phys. Chem. Solid. 120 (2018) 167–172, https://doi.org/10.1016/j.jpcs.2018.04.034.
[12] J. Partanen, P. Backman, R. Backman, M. Hupa, Absorption of HCl by limestone in hot flue gases. Part II: importance of calcium hydroxychloride, Fuel 84 (2005) 1674–1684, https://doi.org/10.1016/j.fuel.2005.02.012.
[13] A.D. Pathak, S. Nedea, H. Zondag, C. Rindt, D. Smeulders, A DFT-based comparative equilibrium study of thermal dehydration and hydrolysis of $CaCl_2$ hydrates and $MgCl_2$ hydrates for seasonal heat storage, Phys. Chem. Chem. Phys. 18 (2016) 10059–10069, https://doi.org/10.1039/c6cp00926c.
[14] H. Cho, J.W. Van Zee, S. Shimpalee, B.A. Tavakoli, J.W. Weidner, B.L. Garcia-Diaz, M.J. Martinez-Rodriguez, L. Olson, J. Gray, Dimensionless analysis for predicting Fe-Ni-Cr alloy corrosion in molten salt systems for concentrated solar power systems, Corrosion 72 (2016) 742–760.
[15] A.K. Galwey, G.M. Laverty, The thermal decomposition of magnesium chloride dihydrate, Thermochim. Acta 138 (1989) 115–127.
[16] J. de Bakker, J. Lamarre, J. Peacey, B. Davis, The phase stabilities of magnesium hydroxychlorides, Metall. Mater. Trans. B Process Metall. Mater. Process. Sci. 43 (2012) 758–763, https://doi.org/10.1007/s11663-012-9673-z.
[17] J. de Bakker, J. Peacey, B. Davis, Thermal decomposition studies on magnesium hydroxychlorides, Can. Metall. Q. 51 (2012) 419–423.
[18] S. Kashani-Nejad, K.W. Ng, R. Harris, Preparation of MgOHCl by controlled dehydration of $MgCl_2 \cdot 6H_2O$, Metall. Mater. Trans. B 35 (2004) 405–406.
[19] S. Kashani-Nejad, K.W. Ng, R. Harris, MgOHCl thermal decomposition kinetics, Metall. Mater. Trans. B Process Metall. Mater. Process. Sci. 36 (2005) 153–157.
[20] Q. Huang, G. Lu, J. Wang, J. Yu, Thermal decomposition mechanisms of $MgCl_2 \cdot 6H_2O$ and $MgCl_2 \cdot H_2O$, J. Anal. Appl. Pyrolysis 91 (2011) 159–164.
[21] H.-C. Eom, H. Park, H.-S. Yoon, Preparation of anhydrous magnesium chloride from magnesium chloride hexahydrate, Adv. Power Technol. 21 (2010) 125–130, https://doi.org/10.1007/s11663-012-9777-5.
[22] Q.-Z. Huang, G.-M. Lu, J. Wang, J.-G. Yu, Mechanism and kinetics of thermal decomposition of $MgCl_2$ x $6H_2O$, Metall. Mater. Trans. B Process Metall. Mater. Process. Sci. 41B (2010) 1059–1066.
[23] B.L. Garcia-Diaz, L. Olson, M. Martinez-Rodriguez, R. Fuentes, H. Colon-Mercado, J. Gray, High temperature electrochemical engineering and clean energy systems, J. South Carolina Acad. Sci. 14 (2016) 11–14.
[24] B.A.T. Mehrabadi, J.W. Weidner, B. Garcia-Diaz, M. Martinez-Rodriguez, L. Olson, S. Shimpalee, Modeling the effect of cathodic protection on superalloys inside high temperature molten salt systems, J. Electrochem. Soc. 164 (2017) C171–C179.
[25] H. Sun, J.Q. Wang, Z. Tang, Y. Liu, C. Wang, Assessment of effects of Mg treatment on corrosivity of molten NaCl-KCl-$MgCl_2$ salt with Raman and infrared spectra, Corrosion Sci. 164 (2020), 108350, https://doi.org/10.1016/j.corsci.2019.108350.
[26] N.B. Zhou, B.Z. Chen, X.K. He, Y.B. Li, Preparation and characteristic research of anhydrous magnesium chloride with dehydrated ammonium carnallite, J. Cent. South Univ. Technol. 13 (2006) 373–378, https://doi.org/10.1007/s11771-006-0051-3 (English Ed.
[27] R.T. Mayes, J. Matthew, K. Phillip, W. Halstenberg, A. McAlister, D. Sulejmanovic, S. Raiman, S. Dai, B. Pint, Purification of Chloride Salts for Concentrated Solar Power Applications, ORNL, 2018.
[28] Z. Zhang, X. Lu, Y. Yan, T. Wang, The dehydration of $MgCl_2 \cdot 6H_2O$ by inhibition of hydrolysis and conversion of hydrolysate, J. Anal. Appl. Pyrolysis 138 (2019) 114–119, https://doi.org/10.1016/j.jaap.2018.12.014.
[29] J.M. Kurley, P.W. Halstenberg, A. McAlister, S. Raiman, S. Dai, R.T. Mayes, Enabling chloride salts for thermal energy storage: implications of salt purity, RSC Adv. 9 (2019) 25602–25608, https://doi.org/10.1039/c9ra03133b.
[30] G.-S. Chen, I.-W. Sun, K.D. Sienerth, A.G. Edwards, G. Mamantov, Removal of oxide impurities from alkali haloaluminate melts using carbon tetrachloride, J. Electrochem. Soc. 140 (1993) 1523–1526, https://doi.org/10.1149/1.2221596.
[31] I.-W. Sun, K.D. Sienerth, G. Mamantov, The use of phosgene for the removal of oxide impurities from a sodium chloroaluminate melt saturated with sodium chloride, J. Electrochem. Soc. 138 (1991) 2850–2852, https://doi.org/10.1149/1.2085328.
[32] G. Brauer, Handbook of Preparative Inorganic Chemistry, second ed., Academic Press, 1963.

[33] H.H. Emons, R. Naumann, T. Pohl, H. Voigt, Thermoanalytical investigations on the decomposition of double salts - I. The decomposition of carnallite, J. Therm. Anal. 29 (1984) 571–579, https://doi.org/10.1007/BF01913466.
[34] R.K. Motkuri, R.S. Vemuri, D. Barpaga, H. Schaef, J.S. Loring, P.F. Martin, D.B. Lao, S.K. Nune, B.P. McGrail, An efficient, solvent-free process for synthesizing anhydrous $MgCl_2$, ACS Sustain. Chem. Eng. 6 (2018) 1048–1054, https://doi.org/10.1021/acssuschemeng.7b03366.
[35] S. Shoval, S. Yariv, The effect of alkali-chloride on the thermal hydrolysis of hydrated magnesium-chloride, Thermochim. Acta 92 (1985) 819–822, https://doi.org/10.1016/0040-6031(85)86003-2.
[36] P.F. Weck, E. Kim, Solar energy storage in phase change materials: first-principles thermodynamic modeling of magnesium chloride hydrates, J. Phys. Chem. C 118 (2014) 4618–4625, https://doi.org/10.1021/jp411461m.
[37] K. Sugimoto, R.E. Dinnebier, J.C. Hanson, Structures of three dehydration products of bischofite from in situ synchrotron powder diffraction data ($MgCl_2{\cdot}nH_2O$; n = 1, 2, 4), Acta Crystallogr. Sect. B Struct. Sci. 63 (2007) 235–242, https://doi.org/10.1107/S0108768107002558.
[38] A. Gutierrez, S. Ushak, M. Linder, High carnallite-bearing material for thermochemical energy storage: thermophysical characterization, ACS Sustain. Chem. Eng. 6 (2018) 6135–6145, https://doi.org/10.1021/acssuschemeng.7b04803.
[39] H.E. Friedrich, B.L. Mordike, Magnesium Technology: Metallurgy, Design Data, Applications, Springer, Berlin, Germany, 2006.
[40] S. Kashani-Nejad, K.W. Ng, R. Harris, Chlorination of MgOHCl with HCl gas, Miner. Process. Extr. Metall. IMM Trans. Sect. C. 115 (2006) 121–122, https://doi.org/10.1179/174328506X91383.
[41] G.L. Haag, Kinetics of the Hydrolysis of $MgCl_2$ and the Chlorination of Magnesia, Iowa State University, 1977.
[42] K.W. Ng, S. Kashani-Nejad, R. Harris, Kinetics of MgO chlorination with HCl gas, Metall. Mater. Trans. B Process Metall. Mater. Process. Sci. 36B (2005) 405–409, https://doi.org/10.1007/s11663-005-0069-1.
[43] N. Klammer, C. Engtrakul, Y. Zhao, Y. Wu, J. Vidal, Method to determine MgO and MgOHCl in chloride molten salts, Anal. Chem. 92 (2020) 3598–3604.
[44] M.R. Gray, P.E. Eaton, T. Le, Kinetics of hydrolysis of chloride salts in model crude oil, Petrol. Sci. Technol. 26 (2008) 1924–1933, https://doi.org/10.1080/10916460701402412.
[45] J.W. McMurray, S.S. Raiman, Thermodynamic modeling of the K-KCl and Mg-$MgCl_2$ binary systems using the CALPHAD method, Sol. Energy 170 (2018) 1039–1042, https://doi.org/10.1016/j.solener.2018.06.013.
[46] A. Komura, H. Imanaga, N. Watanabe, K. Nakanishi, Solubility of magnesium in molten magnesium chloride, J. Soc. Chem. Ind. Jpn. 71 (1968) 1976–1979.
[47] M.A. Bredig, Mixtures of Metals with Molten Salts, 1963.
[48] M. Krumpelt, J. Fischer, I. Johnson, The reaction of magnesium metal with magnesium chloride, J. Phys. Chem. 72 (1968) 506–511, https://doi.org/10.1021/j100848a020.
[49] C.W. Bale, E. Bélisle, P. Chartrand, S.A. Decterov, G. Eriksson, A.E. Gheribi, K. Hack, I. Jung, Y. Kang, J. Melançon, A.D. Pelton, S. Petersen, C. Robelin, J. Sangster, P. Spencer, M. Van Ende, CALPHAD: computer coupling of phase diagrams and thermochemistry FactSage thermochemical software and databases , 2010 – 2016, Calphad 54 (2016) 35–53.
[50] J. Wypartowicz, T. Ostvold, H.A. Oye, The solubility of magnesium metal and the recombination reaction in the industrial magnesium electrolysis, Electrochim. Acta 25 (1980) 151–156.
[51] K.L. Strelets, Chapter XI: electrolysis. Physicochemical properties of the electrolyte, in: Electrolytic Prod. Magnes, 1977, p. 218.
[52] J. Schenin-King, G.S. Picard, Oxoacidity effect on metallic oxide dissolution reactions in fused chlorides, in: Proc. First Eur. Work. Electrochem. Technol. Molten Salts, 1993, pp. 13–22.
[53] W. Ding, A. Bonk, J. Gussone, T. Bauer, Cyclic voltammetry for monitoring corrosive impurities in molten chlorides for thermal energy storage, Energy Procedia 135 (2017) 82–91, https://doi.org/10.1016/j.est.2017.12.007.
[54] X. Wang, Y. Zhao, J.C. Vidal, P. Li, Experimental Study on The Thermal and Transport Properties of A Novel NaCl-KCl-MgCl2 Ternary Molten Salt for Next Generation High Temperature HTF, 2020. In preparation.
[55] T.B. Reed, Free Energy of Formation of Binary Compounds, MIT Press, Cambridge, MA, 1971.
[56] J.C. Vidal, N. Klammer, Molten chloride technology pathway to meet the U.S. DOE SunShot initiative with Gen3 CSP, in: AIP Conf. Proc., Morocco, 2019, https://doi.org/10.1063/1.5117601, 080006.